Challenging Mix Models on Transients to Self-Similarity of Unstably Stratified Homogeneous Turbulence

Benoît-Joseph Gréa[1]
CEA, DAM, DIF,
Arpajon F-91297, France
e-mail: benoit-joseph.grea@cea.fr

Alan Burlot
CEA, DAM, DIF,
Arpajon F-91297, France

Jérôme Griffond
CEA, DAM, DIF,
Arpajon F-91297, France

Antoine Llor
CEA, DAM, DIF,
Arpajon F-91297, France

The present work aims at expanding the set of buoyancy-driven unstable reference flows—a critical ingredient in the development of turbulence models—by considering the recently introduced "Unstably Stratified Homogeneous Turbulence" (USHT) in both its self-similar and transient regimes. The previously established accuracy of an anisotropic Eddy-Damped Quasi-Normal Markovian Model (EDQNM) on the USHT has allowed us to: (i) build a data set of well defined transient flows from Homogeneous Isotropic Turbulence (HIT) to late-time self-similar USHT and (ii) on this basis, calibrate, validate, and compare three common Reynolds-Averaged Navier–Stokes (RANS) mixing models (two-equation, Reynolds stress, and two-fluid). The model calibrations were performed on the self-similar flows constrained by predefined long range correlations (Saffman or Batchelor type). Then, with fixed constants, validations were carried out over the various transients defined by the initial Froude number and mixing intensity. Significant differences between the models are observed, but none of them can accurately capture all of the transient regimes at once. Closer inspection of the various model responses hints at possible routes for their improvement. [DOI: 10.1115/1.4032533]

1 Introduction

The dynamics of buoyancy-driven turbulent flows is difficult to predict since it ensues from complex wave/instability phenomena. Such flows are characterized by a mean gradient of density ρ and an acceleration $g\delta_{i3}$ due to the gravity or the displacement of the system along a vertical direction x_3. If the problem is restricted to incompressible fluids within the Boussinesq limit, it may be viewed as a two-way coupling between the turbulent velocity $\mathbf{u}$ and the buoyancy parameter $\vartheta = g\rho'/(\rho N)$; here, ρ' denotes the density fluctuations and $N = \|g\partial_3\rho/\rho\|^{1/2}$ the characteristic buoyancy frequency usually referred as Brunt-Väisälä frequency for stable configuration ($g\partial_3\rho < 0$). In order to disentangle the different mechanisms at work, the buoyancy frequency N is considered to be independent of the spatial location $\mathbf{x}$ and time t. This is an idealized approach since for realistic flows the gradient of density is not uniform and may evolve in time due to the vertical turbulent mass flux. However, it becomes relevant for turbulent structures small enough compared to the mean stratification scale and for sufficiently small times. An advantage of this idealized case is that statistical homogeneity can be assumed for the fluctuating quantities rendering spectral methods very efficient. It leads to different canonical configurations referred as stably stratified homogeneous turbulence/USHT (SSHT/USHT) [1,2] extending previous homogeneous approaches of Refs. [3–5] in the sense that the density fluctuations are maintained by the presence of the mean density gradient.

Buoyancy-driven turbulence is encountered in many applications related to engineering or geophysics. In particular, SSHT has been the subject of active research for many years since it idealizes many of the situations found in ocean or atmosphere. In contrast, unstably stratified flows akin to the USHT are observed more scarcely due to their transient nature. For this reason, the USHT has attracted less attention despite being a central ingredient to explain important phenomena such as mixing generated by convective down-welling sites in seas [6].

An appealing method in order to explore the properties of buoyancy-driven turbulence consists of looking for self-similar solutions of the flow. The discovery of self-similar solutions in the USHT describing the late time dynamics is quite recent [7,8] and these regimes have not been reached in the experiments of Ref. [9]. However, analogous self-similar solutions have been known for a long time for other homogeneous turbulent flows such as decaying isotropic turbulence [10] or buoyancy induced turbulence without the presence of mean stratification [3]. It is important to stress that all these turbulent flows share an evolution which depends on the initial distribution of energy at large scales. This point is directly related to the question of permanence of big eddies in the HIT. In practice, many theories express this feature by an explicit dependence of the decay or the growth rate on the slope of infrared spectra [11,12].

These aspects go beyond the theoretical questions on idealized problems. The effects of initial conditions on the late-time self-similar regime are a well-known problem in more complex flows such as Rayleigh–Taylor mixing zones (see, for instance, Refs. [13–16]). However, accurate understanding to predict this phenomenon is still missing, despite the many works based on the heuristic approaches such as buoyancy-drag models [17]. Since the USHT shares the same mechanism of baroclinic production of vorticity, it can bring insight to Rayleigh–Taylor turbulence. More precisely, the USHT should properly describe the dynamics structures up to the size of the integral scale at the center of well-developed mixing zones (see Ref. [2]). Also similarly, the USHT can provide a new playground for turbulent mix models dedicated to predict the Rayleigh–Taylor dynamics. It is in fact tempting to test and challenge these models on simple USHT configurations; since simulating these flows is easier, it allows extensive parametric studies and a better understanding of the phenomena.

The objective of this work is thus twofold. In the first step, we explore the different dynamics leading to the self-similar regime in the USHT. Transient patterns and durations display a wide range of behaviors depending on the strength of the mean acceleration applied to the system and the initial state of turbulence.

[1]Corresponding author.

Contributed by the Fluids Engineering Division of ASME for publication in the Journal of Fluids Engineering. Manuscript received March 27, 2015; final manuscript received September 4, 2015; published online April 12, 2016. Assoc. Editor: Daniel Livescu.

These phases are important because in real systems, such as Rayleigh–Taylor, self-similarity is not necessarily reached for instance due to nonconstant acceleration [18,19]. For the present study, we rely on a spectral model recently developed for USHT and based on an anisotropic EDQNM. The results obtained by this approach are very close to direct numerical simulations (DNS) as shown in Ref. [20]. However, direct numerical simulations of USHT are not possible here as we try to avoid finite Reynolds number effects. In the second step, we perform comparisons with different turbulent mix models during transients. This leads us to discuss the common belief that if a turbulent mix model is able to mimic the characteristics of the self-similar solution—such as the growth rate and different anisotropy characteristics—then it can reproduce correctly the dynamics of the flow. For that purpose, we consider three mix models of a very different nature but representative of existing RANS modeling strategies for buoyancy-induced turbulence: two-equation [21], Reynolds stress [22], and two-fluid type [23].

This paper is organized as follows: In Sec. 2, the basic characteristics of USHT and the results from the EDQNM model are exposed with a focus on the transients to self-similarity. Section 3 is dedicated to comparisons with the different mix model as well as the interpretation of the results. Section 4 concludes the paper.

2 The Convergence Toward the Self-Similar Regime in USHT

In this section, the equations and phenomenology of USHT are recalled. We describe the procedure to explore the transients with the EDQNM model, the results are presented afterward.

2.1 Basic Equations of USHT. The equations for USHT can be derived from the incompressible Navier–Stokes equations assuming Boussinesq approximation and a uniform constant mean density gradient along the x_3-vertical component. These equations give the dynamics of the turbulent fluctuations for the velocity $\mathbf{u}(\mathbf{x},t)$, for the reduced pressure $p(\mathbf{x},t)$, and for the buoyancy parameter $\vartheta(\mathbf{x},t)$ as follows:

$$\partial_i u_i = 0 \tag{1a}$$

$$\partial_t u_i + u_j \partial_j u_i = -\partial_i p + \nu \partial_{jj} u_i + N \vartheta \delta_{i3} \tag{1b}$$

$$\partial_t \vartheta + u_j \partial_j \vartheta = \mathcal{D} \partial_{jj} \vartheta + N u_3 \tag{1c}$$

Equation (1*a*) stands for the incompressibility condition, Eqs. (1*b*) and (1*c*) determine the evolution of the velocity and buoyancy parameter, respectively. For convenience, the buoyancy parameter ϑ is rescaled as a velocity by the mean of the buoyancy frequency N, here supposed constant. Also, it can be seen that the frequency N controls the coupling between u_3 and ϑ as already mentioned in Sec. 1. A simple linear analysis reveals the unstable nature of the system. We restrict this study to unit Schmidt number, $\nu = \mathcal{D}$.

Introducing the ensemble average $\langle\ \rangle$, the turbulent quantities correspond to fluctuations with zero mean and we can write $\langle u_i \rangle$, $\langle p \rangle$, $\langle \vartheta \rangle = 0$. The turbulent flow is assumed homogeneous and axisymmetric in the statistical sense. In this USHT problem, anisotropy is fed by the linear buoyancy terms proportional to N.

Equations (1*a*)–(1*c*) can be solved numerically in a cubic box with periodic boundary conditions using classical pseudospectral methods as illustrated in Fig. 1.

These simulations are very convenient tools to study the development of the instability. In particular, one-point quantities such as kinetic energy $\mathcal{K} = \langle u_i u_i \rangle / 2$, variance of buoyancy $\langle \vartheta \vartheta \rangle$ and vertical buoyancy flux $\langle u_3 \vartheta \rangle$ particularly useful for the RANS models can be directly extracted and analyzed. In this study, the initial states of USHT are chosen isotropic, obtained from the decayed HIT simulations. Anisotropic structures for the velocity and the buoyancy parameter appears and grows constantly. This comes along with an increase in the characteristic lengths for energy containing eddies. Therefore, the large scales in USHT become confined while the small ones become under-resolved limiting the possibility of reaching the late time regimes and obtaining very high Reynolds numbers.

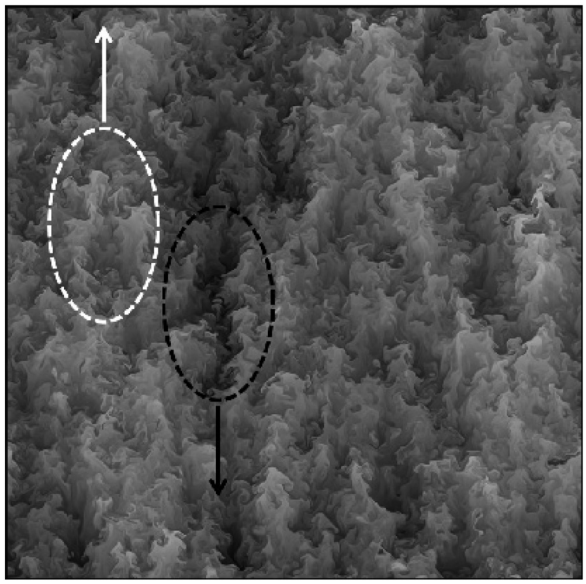

Fig. 1 Visualization of the buoyancy parameter ϑ in a vertical plane of an USHT DNS. The acceleration points to the bottom in the figure. White zones, corresponding to lighter fluid, move upward while heavier darker parcels of fluid move downward.

In USHT, the late time regime becomes self-similar with an exponential growth of turbulent quantities, as $\sim e^{\beta N t}$. This question has been addressed in detail, see, for instance, Refs. [7,20], and [24]. The value of the growth parameter β was shown to depend on s the spectrum slope at large (infrared) scales as $\beta = 4/(s+3)$ (for $s \leq 4$). Accordingly, the growth rate and the anisotropy are larger when for given total energy its distribution is skewed toward larger scales.

2.2 Methodology. In order to investigate the transients and provide reference data for the RANS models, simulations have to:

(1) Start from initial conditions corresponding to a well developed turbulence in order to facilitate the identification of turbulent quantities with the RANS models,
(2) reach the late self-similar regime implying to achieve high Reynolds numbers, and
(3) be fast enough to permit a parametric study on initial conditions.

For this problem, DNS have prohibitive computational cost, and we consider the EDQNM spectral turbulence model described in Ref. [20] to perform the study. One may think to use large eddy simulations (LES) instead to explore transients. LES allows to access the phenomenology of high Reynolds number turbulence [25] under the strong assumption that no bias is introduced by the subgrid model. Still, USHT LES should take into account the growth of the integral scale, typically multiplied by a factor 100 in the cases presented below. It is instructive to evaluate roughly the ratio between the size of the domain and the size of the mesh for the LES of USHT transients. Let us say a ratio of ten is requested between the integral scale and the mesh size for the LES in order to be sufficiently accurate. At the end of the simulation, we need a ratio between the size of the domain and the integral scale of ten to avoid confinement effects which spoil the growth of turbulent quantities. Taking into account the shift of the

integral scale, this leads to a ratio of 10^4 between the size of the domain and the mesh size, therefore necessitating 10^{12} grid points! Needless to say, such LES are very demanding especially for a parametric study.

The presently adapted EDQNM model exploits the spectral representation of turbulence and further aims at including the specific aspects of USHT. The different spectra defined as Fourier transforms of the two-point correlations are written within an axisymmetric formalism. They depend explicitly on the angle between the wave vector and the vertical direction, thus capturing directional anisotropy. The eddy-damping term controlling the dynamics of triple correlations in the model has been enhanced through a dependence on the frequency N to reduce the energy transfer [20]. This aspect may be interpreted as the consequence of sweeping effects between the structures of different buoyancies [26]. The presence of buoyancy production helps closing the eddy-damping term, a delicate and specific problem to USHT. The tractability of the equations results from different simplifications. In addition, the model has a few well-known limitations identified on the isotropic EDQNM models; for instance, a slight underestimation of backscatter effects at large wavenumbers [27] or an underestimation of spectra at small scales attributed to a lack of intermittency phenomenology [28]. Despite these aspects, the model has been able to reproduce accurately one-point statistics from various DNS at moderate Reynolds numbers [20]. At high Reynolds numbers, simulations and experiments are not available and our analysis relies on the solutions of the EDQNM model only. These EDQNM simulations are thus used as our references to evaluate the predictions of classical one-point turbulence models. Clearly, this is a sensitive aspect in our methodology but it has to be kept in mind that EDQNM does take into account the anisotropy and distant interaction effects on the transfer term compared to other, however, very good but more restrictive models, such as in Ref. [29]. At this point, a validation of EDQNM with LES representing high Reynolds number turbulence would be fruitful.

Now, we describe briefly how initial conditions are obtained. At $t=0$ corresponding to the time when buoyancy effects are initiated, the state of turbulence for the simulations is isotropic and homogeneous. It results from a freely decaying turbulence simulation with a passive scalar started at $t<0$. So in practice $N=0$ for $t<0$, and afterward the buoyancy frequency is set at a constant value for $t \geq 0$. The velocity and the buoyancy parameter are decorrelated at $t=0$, i.e., $\langle u_i \vartheta \rangle = 0$. Initial conditions with nonzero anisotropy and vertical buoyancy flux are not considered here because it increases drastically the number of parameters in the system.

It is convenient to characterize the flow with different nondimensional numbers. First, we introduce the turbulent Reynolds number defined from the kinetic energy $\mathcal{K}$, its dissipation $\mathcal{E}$, and the viscosity ν as $\mathrm{Re} = \mathcal{K}^2/\mathcal{E}\nu$. In all the EDQNM simulations proposed, the initial Reynolds number at $t=0$ is $\mathrm{Re}=1000$. In order to fulfill this condition, the Reynolds number is set at higher values at the beginning of the decay phase (for $t<0$). For $\mathrm{Re}=1000$, an inertial range of about one decade can be observed on spectra and viscosity–diffusivity effects at large scales are negligible. This point indicates that, when studying the convergence toward self-similar regime, the results are free from additional effects due to the transition to turbulence [30]. In the simulations presented, the Reynolds numbers increase drastically due to the buoyancy instability up to value of $\mathrm{Re} \sim 10^6$.

The second important parameter is the Froude number, Fr, defined as the ratio between the turbulent and the buoyancy frequency as $\mathrm{Fr} = \mathcal{E}/\mathcal{K}N$. The Froude number compares the buoyancy force to the inertia of turbulent eddies. Depending on its initial value, two different regimes can be identified; on the one hand, when the Froude number is high, buoyancy effects are negligible and the turbulent flow is controlled by the initial freely decaying dynamics of HIT. On the other hand for small initial Froude number, the production of energy due to buoyancy dominates and the flow enters a rapidly accelerated regime [31,32]. Both regimes correspond to a different path toward the final self-similar state and are important to study. In the simulations, we present Froude numbers ranging values from $\mathrm{Fr} \in [0.07, 7.]$.

Finally, we also introduce the mixing parameter Λ, expressing the ratio between fluctuations of buoyancy ϑ and velocity u_i as $\Lambda = \langle \vartheta\vartheta \rangle / \mathcal{K}$. The parameter Λ can take arbitrary values but the presence of buoyancy tends to balance kinetic energy and variance of buoyancy within $\Lambda \in [1.5, 2]$ in the self-similar regime. Therefore, different initial mixing parameters imply different transients. In our study, we consider initial $\Lambda \in [0.15, 20]$. Note that the knowledge of both the initial Froude number Fr and the mixing parameter Λ is enough to characterize the dynamics of the USHT transients and determine initial conditions for the RANS models as the initial vertical buoyancy flux is zero.

As already explained, the initial distribution of energy at large scales is important in USHT as it determines the growth rate of the final self-similar regime. To take this aspect into account, different initial velocity $E(k)$ and buoyancy $B(k)$ spectra depending on the wavenumber k are considered. More precisely, we choose $E(k), B(k) \sim k^s \exp\left[-s(k/k_{\mathrm{peak}})^2/2\right]$ at the beginning of the freely decaying phase ($t<0$). The vertical velocity buoyancy spectrum $F(k)$ remains null during this phase. Integrating spectra over wave number k provides one-point statistics with, in particular, $\mathcal{K} = \int_0^{+\infty} E(k)dk$, $\langle \vartheta\vartheta \rangle = \int_0^{+\infty} B(k)dk$ and $\langle u_3 \vartheta \rangle = \int_0^{+\infty} F(k)dk$. The infrared slope s is taken as 2 (Saffman type) and 4 (Batchelor type) leading to self-similar growth rates β, respectively, of 4/5 and 4/7. The wavenumber value corresponding to the initial maximum of spectra, k_{peak}, is set at 40. During the simulations, wavenumbers corresponding to maxima for the velocity and buoyancy spectra remain nearly the same although slight differences due to nonidentical decay rates of the velocity and the scalar during transients. Also, the value for the viscosity and the diffusion coefficient imposed in all the simulations is $\nu = \mathcal{D} = 5 \times 10^{-5}$.

Around 40 EDQNM simulations are conducted in order to explore the transients to self-similarity. Each simulation has a cost of 10^4 central processing unit hours, reaching Reynolds numbers up to $\mathrm{Re} \sim 10^6$ far beyond the reach of DNS. The different values expressing the initial characteristics of the simulations are shown in Table 1.

2.3 EDQNM Simulated Results. In this section, the characteristics of the transients obtained from the different EDQNM simulations are detailed. In Fig. 2, the time evolution of the Reynolds number, the Froude number, and the mixing intensity

Table 1 Characteristics of the EDQNM simulations at Nt = 0. (Left) With k^2 initial Saffman spectra corresponding to cases S*. (Right) With k^4 initial Batchelor spectra corresponding to cases B*.

Λ\Fr	0.078	0.155	0.31	0.62	3.1
0.184	S1	S6	S11	S16	S21
0.92	S2	S7	S12	S17	S22
1.84	S3	S8	S13	S18	S23
9.2	S4	S9	S14	S19	S24
18.4	S5	S10	S15	S20	S25

Λ\Fr	0.168	0.337	0.670	1.28	6.61
0.181	B1	B4	B7	B10	B13
1.81	B2	B5	B8	B11	B14
18.1	B3	B6	B9	B12	B15

parameter is shown starting from $t=0$ when acceleration is switched on. Initial conditions, as already discussed, derive from different freely decaying states corresponding to $t \leq 0$.

The simulations converge to the self-similar regimes but at a different pace determined by initial conditions. In self-similar regimes, the Reynolds number grows exponentially as $e^{\beta Nt}$, while the Froude number and the mixing parameter are constant. As expected from the theory [8,20], the growth rates are different for k^2 or k^4 infrared spectra. In addition, the asymptotic values for the Froude number are slightly different, with Fr ≈ 0.35 and 0.45 for, respectively, Saffman k^2 and Batchelor k^4 spectra. For similar initial distribution of energy at large scales, the curves for Fr and Λ converge toward the same values. The various features of the transient can be observed more directly on second-order correlations such as the kinetic energy $\mathcal{K}$, the buoyancy variance $\langle \vartheta\vartheta \rangle$, and the vertical buoyancy flux $\langle u_3\vartheta \rangle$ shown in Fig. 3(*a*). The case presented corresponds to S15, and has a small initial Froude number and high initial mixing parameter. The evolutions of the turbulent quantities during the transient (I) contrast with their dynamics during the self-similar regime (II). Also, each quantity does not evolve the same manner despite having the same self-similar behavior. Case S15 is characterized by a strong initial variance of buoyancy compared to kinetic energy so the transient is partly determined by a rebalance of $\mathcal{K}$ compared to $\langle \vartheta\vartheta \rangle$ in this example.

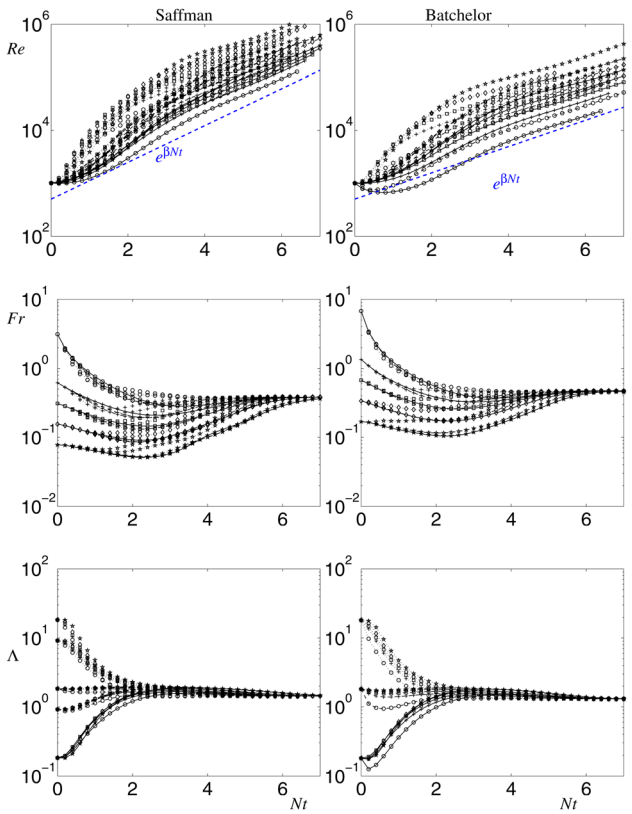

Fig. 2 Evolution of nondimensional numbers as a function of time for the different EDQNM simulations corresponding to Table 1; (top) Reynolds number, (middle) Froude number, (bottom) mixing parameter. (Left) Saffman k^2 spectra with symbols corresponding to initial Froude number; (circle) Fr = 3.1, (cross) Fr = 0.62, (square) Fr = 31, (diamond) Fr = 0.155, and (star) Fr = 0.078. Lines correspond to the initial mixing parameter; (plain) $\Lambda = 0.184$, (dashed) $\Lambda = 0.92$, (dashed–dotted) $\Lambda = 1.84$, (dotted) $\Lambda = 9.2$, and (none) $\Lambda = 18.4$. (right) Batchelor k^4 spectra with symbols corresponding to initial Froude number; (circle) Fr = 6.61, (cross) Fr = 1.28, (square) Fr = 0.67, (diamond) Fr = 0.337, and (star) Fr = 0.168. Lines correspond to initial mixing parameter; (plain) $\Lambda = 18.1$, (dashed) $\Lambda = 1.81$, (dashed–dotted) $\Lambda = 0.184$, and (dotted) $\Lambda = 9.2$.

The initial Froude number being relatively small, buoyancy effects develop quickly and the dynamics of turbulent quantities can be explained from the effect of the linear buoyancy term neglecting all dissipation processes. The rapid acceleration theory (Refs. [31] and [32]) shows that the growth is exponential as $\sim e^{2Nt}$, which is faster than during the late self-similar regime. Regarding spectra, Fig. 3(*b*) illustrates the evolution to self-similar regime accompanied by a growth of the integral scale and diminution of the Kolmogorov scale. An inertial range develops with a classical Kolmogorov–Obhukov $k^{-5/3}$ scaling on $E(k)$ and $B(k)$ and for the vertical buoyancy flux $F(k)$ a trend to $k^{-7/3}$ (see Ref. [8]).

Depending on the initial Froude number, Fr, and the initial mixing parameter Λ, the transients can take different routes. We introduce two characteristic times in order to describe more

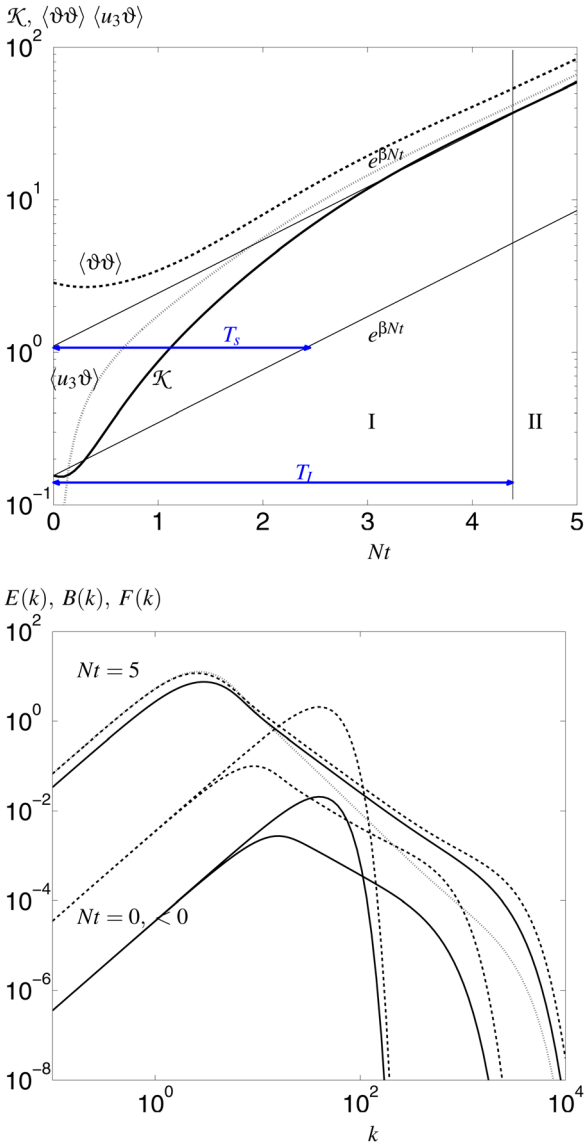

Fig. 3 (Top) Time-evolution of the kinetic energy $\mathcal{K}$ (plain curve), the variance of buoyancy $\langle \vartheta\vartheta \rangle$ (dashed curve) and the vertical buoyancy flux $\langle u_3\vartheta \rangle$ (dotted curve) corresponding to run S15. (Bottom): Energy spectrum $E(k)$ (plain curve), buoyancy spectrum $B(k)$ (dashed curve), and vertical velocity-buoyancy spectrum $F(k)$ (dotted curved) as a function of wavenumber k for run S15. Different times are shown corresponding to the initialization at Nt < 0, when stratification effects are applied Nt = 0 and during self-similar regime $Nt = 5$. $F(k)$ is nonzero only for $t > 0$.

precisely these dynamics. First, the transition delay T_I corresponds to the instance such that the growth rate of the kinetic energy, $\mathcal{K}$, remains close to 10% of its theoretical asymptotic value β. This can be expressed as

$$T_I = \min_t \left\{ \forall t' \geq t, \quad \text{we have} \ \frac{\left\| \beta - \frac{1}{\mathcal{K}} \frac{d\mathcal{K}}{dNt}(t') \right\|}{\beta} \leq 0.1 \right\} \tag{2}$$

In addition, we define the time T_s corresponding to the temporal gap between the self-similar solution and a virtual self-similar solution passing through the initial value of kinetic energy $\mathcal{K}(t=0)$ (see Fig. 3). This is obtained by

$$T_s = \frac{\log(\mathcal{K}(t=T_I)) - \log(\mathcal{K}(t=0))}{\beta N} - T_I \tag{3}$$

Therefore, the sign of T_s indicates if during the transients the growth rate is stronger (>0) or smaller (<0) in average than during the self-similar phase. The couple T_I and T_s provides a simplified but fair description of the transients to the self-similar regime. Now, it is possible to represent these times as a function of initial Froude and mixing parameter as in Figs. 4 and 5. These figures show that the transient is very sensitive to the initial Froude number, and to a lesser degree to the mixing parameter. For Fr $\gg$ 1, the turbulence decays freely until buoyant effects are strong enough to rule the dynamics of the flow. On the contrary, for Fr $\ll$ 1, the turbulence is driven by rapid acceleration theory characterized by an important growth rate $\beta = 2$. For these two opposite regimes, the duration of the transition delay T_I is increased but depending on the time shift is decreased (Fr $\gg$ 1) or increased (Fr $\ll$ 1). The effects of the mixing parameter seem second-order compared to the influence of the Froude number. In fact, Λ converges very rapidly to its asymptotic value while Fr controls the final evolution to self-similarity as indicated in Fig. 2.

3 Modeling the Transients

In this section, we study how the different one-point turbulence models are able to reproduce the behavior of the transients described in Sec. 2. We start by introducing the models, we explain how the model coefficients are adjusted to the self-similar regime, and how the models are initialized. Then, we compare the models with the EDQNM simulations and discuss the implications for the different closures.

3.1 Presentation of the One-Point Turbulence Models for Buoyancy Induced Mixing

3.1.1 $\mathcal{K}-\mathcal{E}$ Mix Model. One of the simpler and older RANS models which can account for buoyancy effects is the two-equation $\mathcal{K}-\mathcal{E}$ model described in Ref. [21]. Its dynamics is

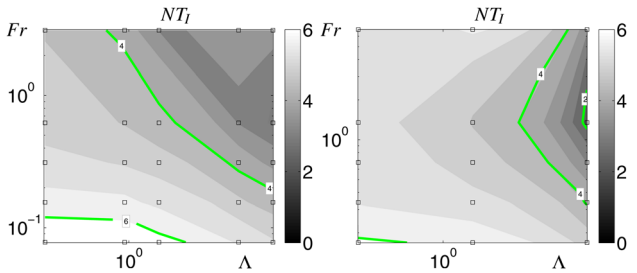

Fig. 4 Nondimensional transition delay NT_I as a function of initial Froude and mixing parameter and obtained from Eq. (2) for the k^2 Saffman spectra. The square symbols correspond to the simulations points of Table 1.

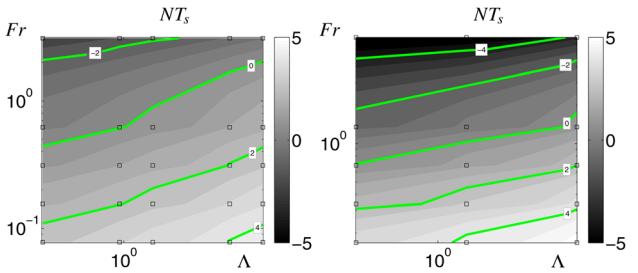

Fig. 5 Nondimensional time shift NT_s as a function of initial Froude and mixing parameter and obtained from Eq. (2) for the k^4 Batchelor spectra. The square symbols correspond to the simulations points of Table 1.

given by the following system of equations for kinetic energy and its dissipation here adapted to the USHT configuration

$$\frac{d}{dt}\mathcal{K} = aN^2 \frac{\mathcal{K}^2}{\mathcal{E}} - \mathcal{E} \tag{4a}$$

$$\frac{d}{dt}\mathcal{E} = aN^2 C_{\varepsilon 0}\mathcal{K} - C_{\varepsilon 2}\frac{\mathcal{E}^2}{\mathcal{K}} \tag{4b}$$

In the equations for $\mathcal{K}$ and $\mathcal{E}$, Eqs. (4*a*) and (4*b*), the first terms on the right-hand side which are proportional to N^2 correspond to the production of energy due to buoyancy effects, and the last ones refer to the dissipation process. The $\mathcal{K}-\mathcal{E}$ model cannot describe the effects of the mixing parameter as it does not contain the variance of buoyancy. Also, since the model relies on first gradient closures, the vertical mass flux is implicitly supposed to be proportional to $\mathcal{K}^2/\mathcal{E}$.

The model contains three coefficients a, $C_{\varepsilon 0}$, $C_{\varepsilon 2}$ which need to be adjusted. Two sets of coefficients specifically adapted to the different kinds of EDQNM simulations (Saffman and Batchelor) are proposed. We start by determining $C_{\varepsilon 2}$ in order to have the correct self-similar decay rate of HIT. In this regime, the kinetic energy evolves as $\mathcal{K} \sim t^{-n}$ with $n = 6/5$ for a Saffman energy spectrum and $n = 10/7$ for Batchelor spectrum. Then, the remaining coefficients a, $C_{\varepsilon 0}$ are provided by the self-similar growth rate and Froude number in USHT, with $\beta = 4/5$ and Fr ≈ 0.35 for Saffman spectra and with $\beta = 4/7$, Fr ≈ 0.45 for Batchelor spectra. The different values of the coefficients used for the comparisons with EDQNM are presented in Table 2. Here, the coefficients proposed are purely designed for the USHT test cases and differ sensitively from classical values. For instance, $C_{\varepsilon 2}$ usually takes higher values adjusted on the experimental measurement of grid turbulence decay. Also, lower values are often considered for $C_{\varepsilon 0}$ and $a(=C_\mu/\sigma_\rho)$ (see Ref. [33]). Nevertheless, the values of the $C_{\varepsilon 0} \sim 0.8$ and $a \sim 0.5$ measured in Rayleigh–Taylor DNS (Refs. [34–36]) are not compatible with the asymptotic growth rate of the mixing zone. This suggests that the model performs very poorly on USHT as will be seen below.

For the initialization procedure, it is enough to use directly the values of Fr obtained from the EDQNM simulations at $t = 0$. Note the model cannot represent the mixing parameter Λ.

Table 2 Coefficients used in the $\mathcal{K}-\mathcal{E}$ model for Batchelor and Saffman initial spectra cases

Case	$C_{\varepsilon 0}$	$C_{\varepsilon 2}$	a
Batchelor	1.308	1.7	0.459
Saffman	1.252	1.83	0.4025

Table 3 Coefficients used in the GSG+ model for Batchelor and Saffman initial spectra cases

Case	$C_{\varepsilon 0}$	$C_{\varepsilon 2}$	C_{u2}	$C_{\rho 2}$	γ	C_1
Batchelor	1.31	1.7	3.4	2.11	0.33	1.8
Saffman	1.28	1.83	2.96	1.65	0.33	1.79

Table 4 Coefficients used in the 2SFK model for Batchelor and Saffman initial spectra cases

Case	C_a	C_{ec}	C_{e1}	$C_{\varepsilon 2}$	C_d
Batchelor	0.5	2	1.5	1.7	1.33
Saffman	0.5	2	1.5	1.83	1.6

3.1.2 Reynolds Stress Model GSG+. The Reynolds stress model GSG+ (see Refs. [22] and [37]) describes the dynamics of second-order correlations and the dissipation. In its Boussinesq formulation, GSG+ is also very similar to BHR3 [38]. We study here its dynamics in the USHT configuration. The different equations standing for, respectively, the correlations of the vertical and horizontal velocities, the velocity/buoyancy cross correlation, the variance of buoyancy, and the dissipation of kinetic energy can be written as

$$\frac{d}{dt}\langle u_3u_3\rangle = 2\left(1-\frac{2}{3}\gamma\right)N\langle u_3\vartheta\rangle - C_1\frac{\mathcal{E}}{\mathcal{K}}\left(\langle u_3u_3\rangle - \frac{2}{3}\mathcal{K}\right) - \frac{2}{3}\mathcal{E} \tag{5a}$$

$$\frac{d}{dt}\langle u_hu_h\rangle = \frac{2}{3}\gamma N\langle u_3\vartheta\rangle - C_1\frac{\mathcal{E}}{\mathcal{K}}\left(\langle u_hu_h\rangle - \frac{2}{3}\mathcal{K}\right) - \frac{2}{3}\mathcal{E} \tag{5b}$$

$$\frac{d}{dt}\langle u_3\vartheta\rangle = N\langle u_3u_3\rangle + (1-\gamma)N\langle\vartheta\vartheta\rangle - C_{u2}\frac{\mathcal{E}}{\mathcal{K}}\langle u_3\vartheta\rangle \tag{5c}$$

$$\frac{d}{dt}\langle\vartheta\vartheta\rangle = 2N\langle u_3\vartheta\rangle - C_{\rho 2}\frac{\mathcal{E}}{\mathcal{K}}\langle\vartheta\vartheta\rangle \tag{5d}$$

$$\frac{d}{dt}\mathcal{E} = C_{\varepsilon 0}\frac{\mathcal{E}}{\mathcal{K}}N\langle u_3\vartheta\rangle - C_{\varepsilon 2}\frac{\mathcal{E}^2}{\mathcal{K}} \tag{5e}$$

At the right-hand sides of Eqs. (5*a*)–(5*e*) appear the production due to buoyancy proportional to N, the term of return to isotropy proportional to the constant C_1, and the different dissipations. The kinetic energy is divided between the vertical and the horizontal components as $\mathcal{K} = \langle u_3u_3\rangle/2 + \langle u_hu_h\rangle$ (we use subscript $h = 1, 2$ for convenience). The redistribution of energy due to the rapid pressure effects are closed through the terms proportional to γ.

The coefficients used for the comparisons with the EDQNM simulations are presented in Table 3, with also two sets corresponding to Saffman and Batchelor long-range initial correlations. As for the two-equation $\mathcal{K}-\mathcal{E}$ model, these coefficients ensure that the self-similar decay rate n and growth rate β correspond to the theoretical values predicted for Saffman and Batchelor spectra. The coefficient γ takes the value one-third in order to capture the correct initial evolution of turbulent quantities during a rapid acceleration phase starting from an isotropic state. Other constraints come from the self-similar regime of USHT in order to get the asymptotic Froude number, the anisotropy of the Reynolds stress and mixing parameter obtained by EDQNM simulations.

All the turbulent quantities described by the Reynolds stress model can be initialized directly at $t = 0$ from the different EDQNM spectra.

3.1.3 Two-Structure Two-Fluid Model 2SFK. We consider the two-structure two-fluid model 2SFK which is described in Ref. [23]. In the 2SFK model, the dynamics of buoyancy-induced turbulence comes from the interaction between rising and descending structures of different densities. For the USHT flow, the model leads to a system of equations for the contrast of buoyancy $\delta\vartheta$ and vertical velocity difference δu between structures, the turbulent kinetic energy inside the structures $\mathcal{K}^*$, and the total dissipation of turbulent kinetic energy $\mathcal{E}$, which reads

$$\frac{d}{dt}\delta\vartheta = N\delta u - \frac{C_{ec}}{4}\frac{\mathcal{E}}{\mathcal{K}^*}\delta\vartheta \tag{6a}$$

$$\frac{d}{dt}\delta u = \frac{1}{(1+C_a)}N\delta\vartheta - \frac{1}{4}\frac{C_d}{(1+C_a)}\frac{\mathcal{E}}{\mathcal{K}^*}\delta u \tag{6b}$$

$$\frac{d}{dt}\mathcal{K}^* = \frac{1}{16}C_d\frac{\mathcal{E}}{\mathcal{K}^*}\delta u^2 - \mathcal{E} \tag{6c}$$

$$\frac{d}{dt}\mathcal{E} = C_{e1}\frac{1}{16}C_d\left(\frac{\mathcal{E}}{\mathcal{K}^*}\right)^2\delta u^2 - C_{\varepsilon 2}\frac{\mathcal{E}}{\mathcal{K}^*}\mathcal{E} \tag{6d}$$

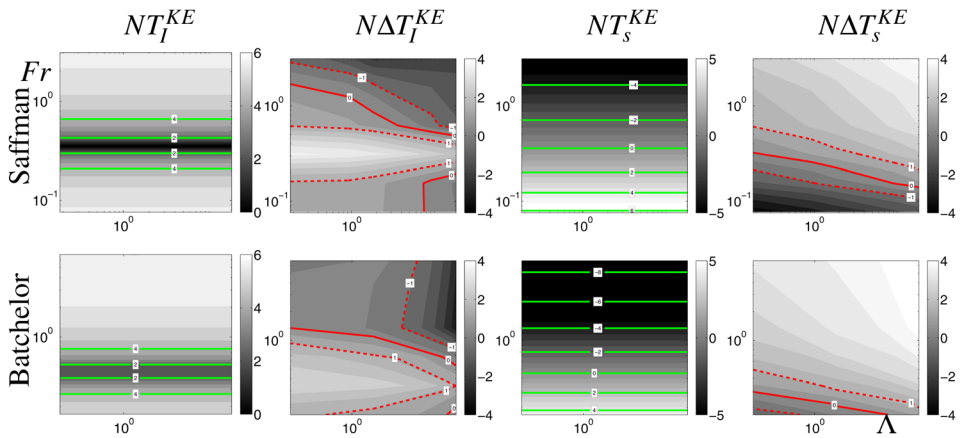

Fig. 6 Transition delays T_l^{KE} and time shifts T_s^{KE} as a function of the initial mixing parameter Λ (abscissa) and the Froude number Fr (ordinate) obtained from Eqs. (2) and (3) for the $\mathcal{K}-\mathcal{E}$ model. Also, the differences between EDQNM and the $\mathcal{K}-\mathcal{E}$ model on transition delays $\Delta T_l^{KE} = T_l - T_l^{KE}$ and on time shifts $\Delta T_s^{KE} = T_s - T_s^{KE}$ are represented. Cases for Saffman (top) and Batchelor (bottom) initial spectra are represented.

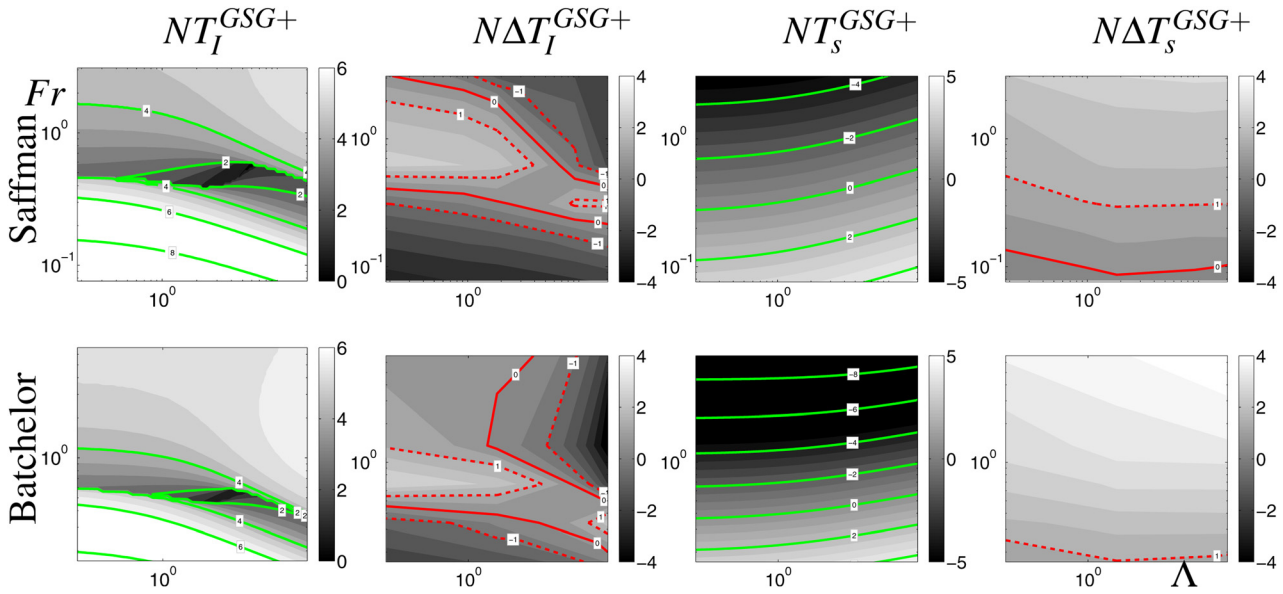

Fig. 7 Transition delays T_I^{GSG+} and time shifts T_s^{GSG+} as a function of the initial mixing parameter Λ (abscissa) and the Froude number Fr (ordinate) obtained from Eqs. (2) and (3) for the RSM GSG+ model. Also, the differences between EDQNM and the GSG+ model on transition delays $\Delta T_I^{GSG+} = T_I - T_I^{GSG+}$ and on time shifts $\Delta T_s^{GSG+} = T_s - T_s^{GSG+}$ are represented. Cases for Saffman (top) and Batchelor (bottom) initial spectra are represented.

In the 2SFK model, the buoyancy production terms proportional to N increase the contrasts of buoyancy and velocity between structures. This effect is counterbalanced by the terms of buoyancy exchange and drag force, respectively, proportional to C_{ec} and C_d, which transfer interstructure density contrast and directed–added mass energy to intrastructure fluctuations and turbulence. The coefficient C_a is associated with added mass effects, accounting for the pressure effects. The energy inside the structures is dissipated at small scales by $\mathcal{E}$. Note that in this model, the different exchange terms are determined by the turbulent frequency of the large in-structure eddies, $\mathcal{E}/\mathcal{K}^*$ accounting for smaller turbulent eddies. The total turbulent kinetic energy of the system is related to the drift velocity δu and $\mathcal{K}^*$ by $\mathcal{K} = \mathcal{K}^* + (1 + C_a)\delta u^2/8$. In addition, the vertical component of the Reynolds stress tensor is provided by $\langle u_3 u_3 \rangle = 2\mathcal{K}^*/3 + (1 + C_a/3)\delta u^2/4$ in 2SFK. This comes from the fact that the kinetic energy inside the structures $\mathcal{K}^*$ and the energy accounted for by the added mass C_a are assumed isotropic while the directed energy $\delta u^2/8$ is purely oriented along the vertical direction.

The adjusted coefficients for the 2SFK model are shown in Table 4.

As for the other models, these coefficients ensure the correct self-similar rates of both HIT decay and USHT growth rates, for Saffman and Batchelor spectra. The added mass coefficient is

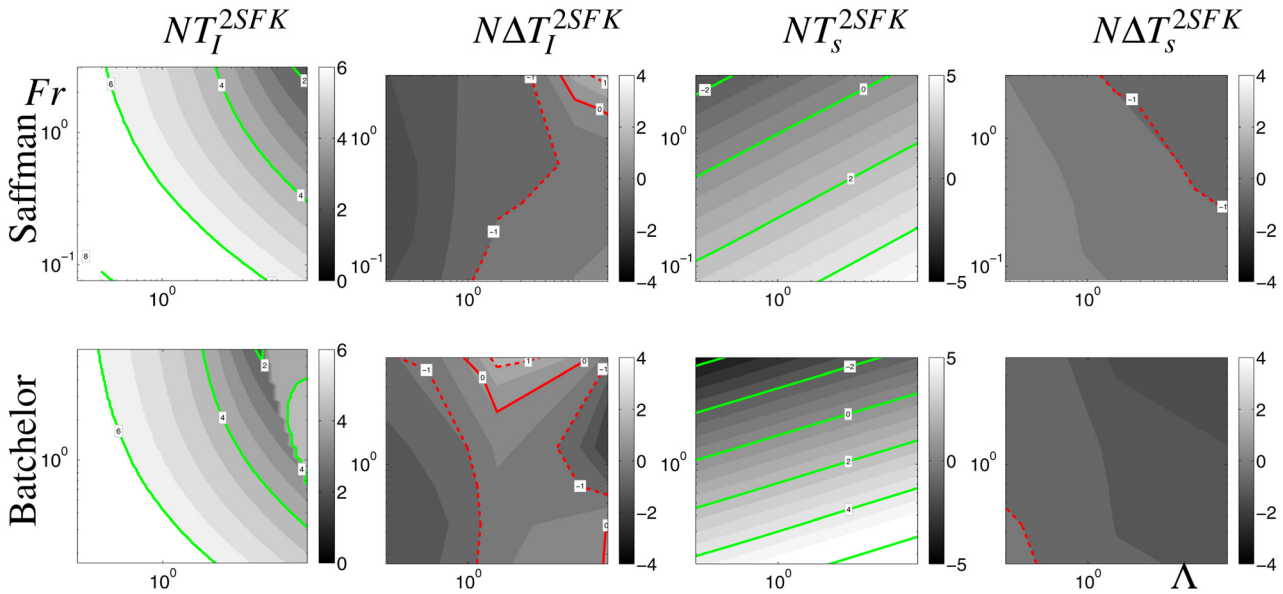

Fig. 8 Transition delays T_I^{2SFK} and time shifts T_s^{2SFK} as a function of the initial mixing parameter Λ (abscissa) and the Froude number Fr (ordinate) obtained from Eqs. (2) and (3) for the 2SFK model. Also, the differences between EDQNM and the 2SFK model on transition delays $\Delta T_I^{2SFK} = T_I - T_I^{2SFK}$ and on time shifts $\Delta T_s^{2SFK} = T_s - T_s^{2SFK}$ are represented. Cases for Saffman (top) and Batchelor (bottom) initial spectra are represented.

chosen to be $C_a = 0.5$, the typical value for spheres. In USHT, this coefficient plays the same role as γ in the GSG+ model.

In order to initialize the 2SFK model from the isotropic conditions at $t = 0$, we take $\delta u = 0$ and $\mathcal{K}^* = \mathcal{K}$. Because $\delta\vartheta$ accounts for only one part of the density fluctuations—which, without explicit structure field equations, cannot be obtained in the present state of the EDQNM simulations—we have assumed an identical half-to-half ratio of inter- to intra-structure fluctuations as in previously performed DNS of self-similar Rayleigh–Taylor flow [39]. The interstructure variance of buoyancy being $(\delta\vartheta/2)^2$, we thus set $\delta\vartheta = (2\langle\vartheta\vartheta\rangle)^{1/2}$ but tests have shown low sensitivity to this ratio.

3.2 Results and Discussion. In order to study the transients toward the final regime of USHT for the different RANS models, we introduce similarly to Sec. 2.3 the transition delays and time shifts $T^*_{I,s}$, with $*$ standing for KE, GSG+, or 2SFK, using the same formulas, Eqs. (2) and (3). For each model, we represent the different times as a function of the Froude number and the mixing parameter in Figs. 6–8. The discrepancy with the EDQNM model can be evaluated by introducing the quantities, $\Delta T^*_{I,s} = T^*_{I,s} - T_{I,s}$. The positive or negative sign of $\Delta T^*_{I,s}$ indicates a shorter or longer model transient, respectively, and a smaller or stronger average growth rate during transients compared to the EDQNM simulations. Therefore, if $\Delta T^*_{I,s} \approx 0$ for some initial conditions, the model is relatively close to the EDQNM solution.

In parallel, we show in Figs. 9–12, the evolution of kinetic energy and Froude number for the models on the different cases with initial Saffman or Batchelor spectra. In fact, kinetic energy and Froude number (which gives the dissipation here) are the only variables commonly described by the various models.

Despite being adjusted on the self-similar USHT solutions, the differences with the EDQNM reference can be very important during the transients. Depending on some initial conditions, we find regions where $|\Delta T^*_I|$, $|\Delta T^*_s| \geq 2$ for the $\mathcal{K} - \mathcal{E}$, GSG+, and 2SFK models.

Clearly, the perfect knowledge of the final characteristics of the flow and of the initial state of turbulence does not guarantee good predictions. Also, the complexity of a model does not necessarily imply more satisfactory results. For instance, the $\mathcal{K} - \mathcal{E}$ model at moderate Froude number and at small mixing parameter (case S11 in Fig. 9 for instance) looks better than GSG+ or 2SFK as it returns accurate values of T_I and T_s. However, in vast regions of the Λ –Fr plane, the $\mathcal{K} - \mathcal{E}$ model performs very poorly compared to the others.

Furthermore, we review in detail the behaviors of different models during the transients:

The $\mathcal{K} - \mathcal{E}$ model cannot account for the variance of buoyancy and the results in Fig. 6 show no dependence on the Λ parameter. However, the global effect of Froude number is qualitatively correct with a transition delay increasing for $\mathrm{Fr} \gg 1$ or $\mathrm{Fr} \ll 1$ corresponding to a decay or an enhanced growth as shown by the time shift. For a specific value of the initial Froude number, the transition delay drops to zero as the model is already in its self-similar regime. This situation is obviously nonphysical as the vertical buoyancy flux is nonzero in the self-similar regime but not in the initial isotropic state. Perhaps, one of the most important failures of the model is when the Froude number is very small, corresponding to a rapid acceleration phase: this phenomenon induces a great sensitivity to initial conditions but can be reduced by decreasing the transition delay with $C_{\varepsilon 0} = 1.5$ as previously suggested [40].

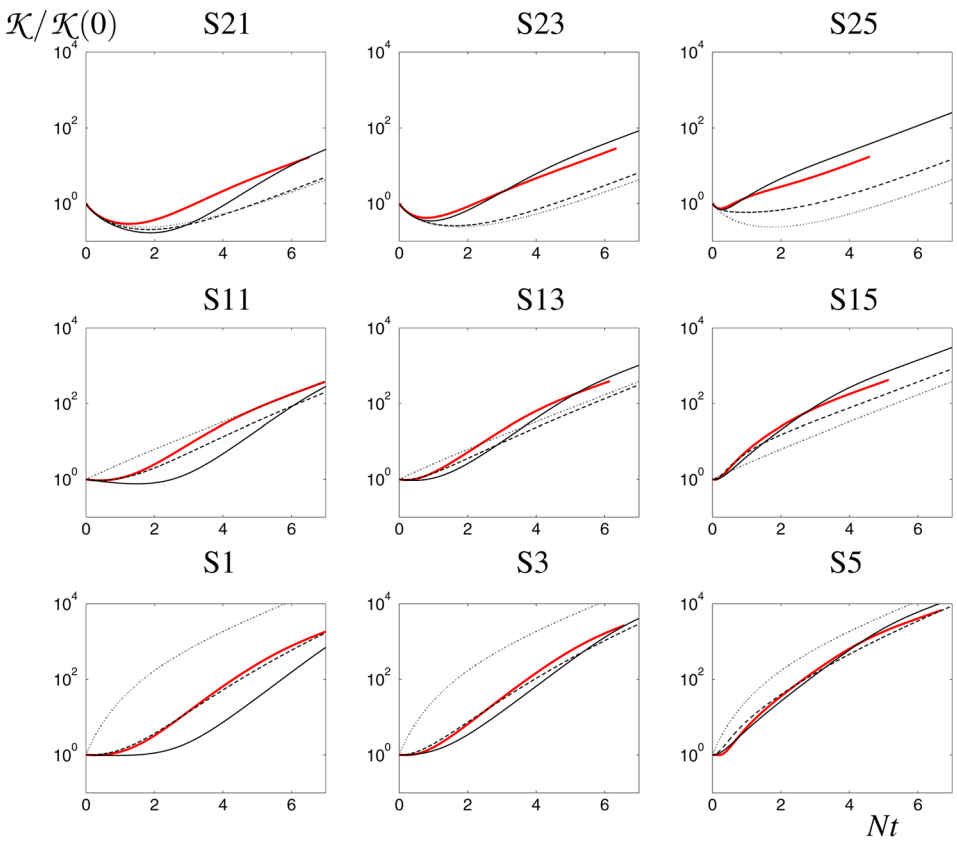

Fig. 9 Evolution of the kinetic energy $\mathcal{K}$ as a function of time Nt for different cases S* with Saffman initial spectra. (Thick red plain line) EDQNM, (thin plain line) 2SFK, (dashed line) GSG+, and (dotted line) $\mathcal{K}-\mathcal{E}$.

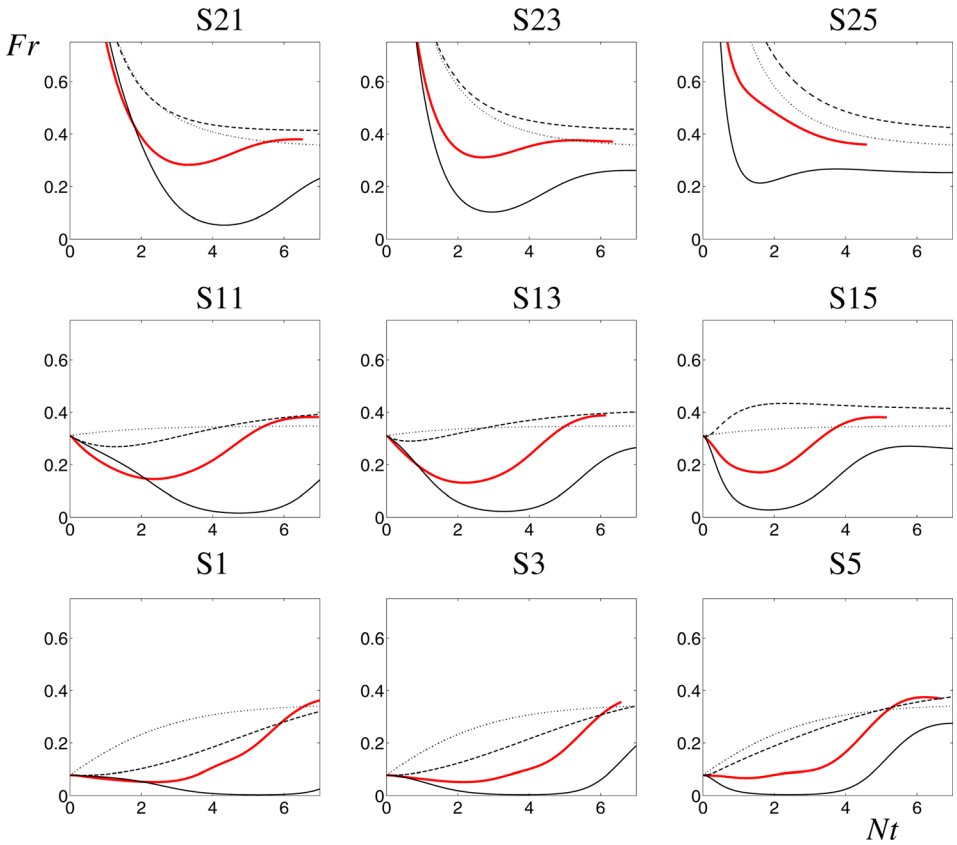

Fig. 10 Evolution of the Froude number Fr = $\mathcal{E}/\mathcal{K}N$ as a function of time Nt for different cases S* with Saffman initial spectra. (Thick red plain line) EDQNM, (thin plain line) 2SFK, (dashed line) GSG+, and (dotted line) $\mathcal{K}-\mathcal{E}$.

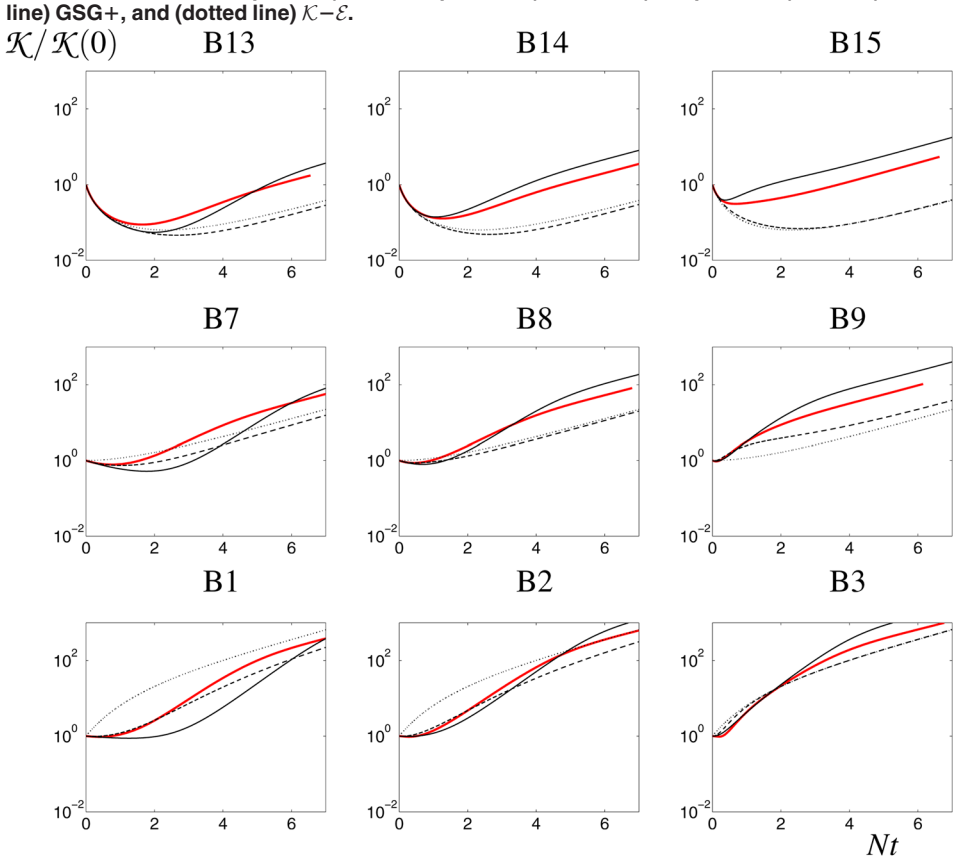

Fig. 11 Evolution of the kinetic energy $\mathcal{K}$ as a function of time Nt for different cases B* with Batchelor initial spectra. (Thick red plain line) EDQNM, (thin plain line) 2SFK, (dashed line) GSG+, and (dotted line) $\mathcal{K}-\mathcal{E}$.

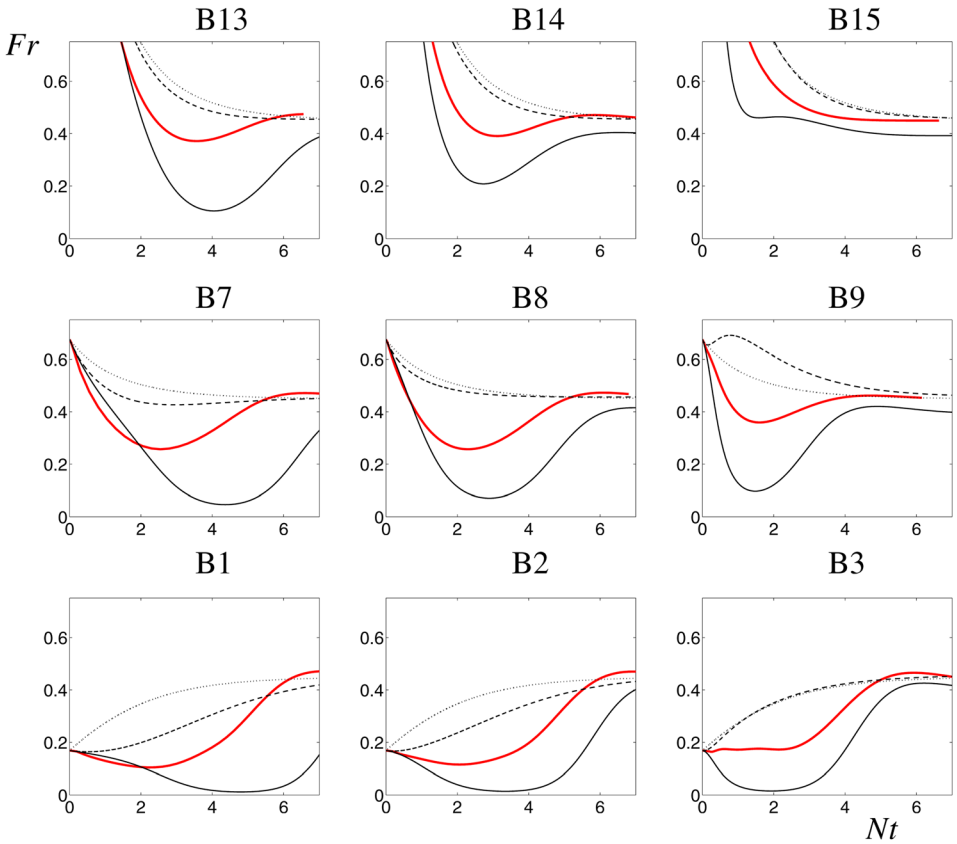

Fig. 12 Evolution of the Froude number Fr = $\mathcal{E}/\mathcal{K}N$ as a function of time Nt for different cases B* with Batchelor initial spectra. (Thick red plain line) EDQNM, (thin plain line) 2SFK, (dashed line) GSG+, and (dotted line) $\mathcal{K}-\mathcal{E}$.

The Reynolds stress model GSG+ performs very well at short times (Nt $\leq$ 1) as it has been adjusted on rapid acceleration regime starting from isotropic states (see Figs. 9 and 11). However, the final capture of the transients is a bit disappointing as there is a clear underestimation of the production of kinetic energy compared to the EDQNM simulations as shown by the positive values of ΔT_s^{GSG+} in Fig. 7. Note that using a different strategy to calibrate the coefficients of the model does not seem to improve the predictions. This point can be explained by a distorted evolution for the turbulent frequency as shown in Figs. 10 and 12. The turbulent frequency controls the dissipation terms in the equations for the different correlations and seems to be overestimated by the GSG+ model. As a result, the vertical buoyancy flux is underestimated as shown in Fig. 13 (corresponding to case S23) leading to a poor capture of kinetic energy production and an unbalance in the ratio between kinetic energy and buoyancy variance (as expressed by Λ in Fig. 13). In the USHT transients, turbulence is very unsteady and there is no equilibrium between the production of energy due to buoyancy at large scales and the nonlinear transfer of energy to small scales where dissipation dominates. Therefore, the turbulent frequency in GSG+ constructed from dissipation, but not the energy flux at large scales, cannot properly represent the transfer of energy at large scales. An appealing solution in order to improve the model consists of considering a two-scale RSM model [41].

The 2SFK model behaves very differently from the RSM model. It performs very well for moderate or high mixing parameter Λ. In fact, the initial evolution of the turbulent frequency is correct as kinetic energy increases due to production but the dissipation needs time to evolve till the energy reaches small scales. This effect is well reproduced in 2SFK as the energy is not dissipated directly by the drag force between structures but transferred to the intrastructure kinetic energy $\mathcal{K}^*$ which corresponds to smaller eddies. However, 2SFK presents a serious limitation for small Λ values as the evolution of kinetic energy at short time is clearly underestimated. In fact, if initially the difference velocity δu and the contrast of buoyancy $\delta\vartheta$ are simultaneously zero (corresponding to small Λ), the model is unable to evolve even if the turbulent kinetic energy is important in $\mathcal{K}^*$. This effect can be corrected by adding a source term in the equation for $\delta\vartheta$ depending on $\mathcal{K}^*$ as turbulent agitation would generate contrast of buoyancy between the structures.

Where do the qualitative differences between the models come from? After a close examination, it can be traced back to the specificities of the dissipation equation. In any case, from an energy equation $d\mathcal{K}'/dt = \Pi - \mathcal{E}$ where production Π and dissipation $\mathcal{E}$ are balanced, the time derivative of the dissipation $\mathcal{E}$ is postulated from dimensional reasoning by multiplying that of $\mathcal{K}'$ by a turbulent frequency and inserting a free coefficient for each term leading to the form $d\mathcal{E}/dt = C_{\Pi}\mathcal{E}/\mathcal{K}'\Pi - C_{\varepsilon 2}\mathcal{E}/\mathcal{K}'\mathcal{E}$.

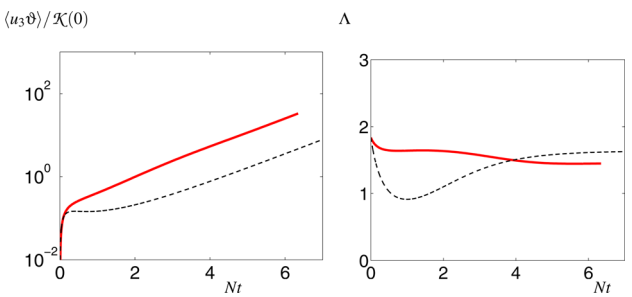

Fig. 13 (Left) Evolution of the vertical buoyancy flux $\langle u_3\vartheta\rangle$, (right) evolution of the mixing parameter Λ as a function of time Nt for the S23 case. (Thick red plain line) EDQNM and (dashed line) GSG+.

On the one hand, the $\mathcal{K}-\mathcal{E}$ and GSG+ mix models start from the total kinetic energy, which means that they take $\mathcal{K}' = \langle u_i u_i \rangle/2$. On the other hand, the choice of 2SFK is to take only a fraction of the total kinetic energy, which is the energy inside the structures $\mathcal{K}' = \mathcal{K}^*$. The fraction is large at the beginning of the simulations due to the choice of the initial condition but it becomes smaller in the self-similar regime. Furthermore, the Π term in 2SFK does not directly react to buoyant production like in GSG+ but appears as a transfer term from the interstructure energy to the inner structure energy. This delays the effect of buoyancy production on the dissipation qualitatively in accordance with EDQNM.

On the contrary, with $\mathcal{K}-\mathcal{E}$ and GSG+, the buoyant production occurring at large scales instantaneously increases the dissipation though the latter is effective at small scales. This limitation can be alleviated following the ideas of two scale models [41] where at least an additional variable related to the energy transfer is added. The production contributing to large-scale energy must be transferred to the small-scale energy through this variable before it can influence the dissipation growth.

4 Conclusion

In this work, an exploration of the transients to self-similar regimes of USHT is presented. To this end, the anisotropic EDQNM spectral model described in Ref. [20] has been used. The data obtained are free from transition to turbulence and low Reynolds number effects, reach very high Reynolds number values, and cover a large panel of initial conditions. Accordingly, they could not have been obtained by actual DNS. A particular emphasis is given to the influence of the initial Froude number and initial mixing parameter on the flow evolution. The results are used as references to validate the solutions of the two-equation $\mathcal{K}-\mathcal{E}$ model, the Reynolds stress model GSG+, and the two-structure two-fluid model 2SFK adjusted to return the final self-similar states of USHT. The comparisons establish clearly that the knowledge of the self-similar regime and initial state of turbulence is not sufficient to guarantee good predictions. However, this study allows to identify different missing elements of physics in one-point turbulence model and their improvement. In particular, a model performing well on USHT must:

(1) Capture the linear two-way coupling between velocity and buoyancy controlling the short time dynamics during rapidly accelerated phases.
(2) Take into account some nonequilibrium mechanisms in the dissipation equation; during transients, the turbulent energy produced at large scales differs from the transfer to small scales where energy is destructed.

Beyond these aspects, we contend the idea that validating mix models on transients can supplement the standard strategies based on the self-similar regimes or experiments presented in Refs. [38] and [42].

References

[1] Godeferd, F. S., and Cambon, C., 1994, "Detailed Investigation of Energy Transfers in Homogeneous Stratified Turbulence," Phys. Fluids, **6**(6), pp. 2084–2100.
[2] Griffond, J., Gréa, B. J., and Soulard, O., 2014, "Unstably Stratified Homogeneous Turbulence as a Tool for Turbulent Mixing Modeling," ASME J. Fluids Eng., **136**(9), p. 091201.
[3] Batchelor, G. K., Canuto, V. M., and Chasnov, J. R., 1992, "Homogeneous Buoyancy-Generated Turbulence," J. Fluid Mech., **235**(2), pp. 349–378.
[4] Livescu, D., and Ristorcelli, J. R., 2007, "Buoyancy-Driven Variable-Density Turbulence," J. Fluid Mech., **591**(11), pp. 43–71.
[5] Chung, D., and Pullin, D., 2009, "Direct Numerical Simulation and Large-Eddy Simulation of Stationary Buoyancy-Driven Turbulence," J. Fluid Mech., **643**, pp. 279–308.
[6] Lazier, J., Hendry, R., Clarke, A., Yashayaev, I., and Rhines, P., 2002, "Convection and Restratification in the Labrador Sea, 1990–2000," Deep Sea Res. Part I: Oceanogr. Res. Pap., **49**(10), pp. 1819–1835.
[7] Soulard, O., Griffond, J., and Gréa, B.-J., 2014, "Large-Scale Analysis of Self-Similar Unstably Stratified Homogeneous Turbulence," Phys. Fluids, **26**(1), p. 015110.
[8] Burlot, A., Gréa, B.-J., Godeferd, F. S., Cambon, C., and Soulard, O., 2015, "Large Reynolds Number Self-Similar States of Unstably Stratified Homogeneous Turbulence," Phys. Fluids, **27**(6), p. 065114.
[9] Thoroddsen, S. T., Van Atta, C. W., and Yampolsky, J. S., 1998, "Experiments on Homogeneous Turbulence in an Unstably Stratified Fluid," Phys. Fluids, **10**(12), pp. 3155–3167.
[10] Batchelor, G. K., 1949, "The Role of Big Eddies in Homogeneous Turbulence," Proc. R. Soc. London, Ser. A, **195**(1043), pp. 513–532.
[11] Llor, A., 2011, "Langevin Equation of Big Structure Dynamics in Turbulence: Landaus Invariant in the Decay of Homogeneous Isotropic Turbulence," Eur. J. Mech. B/Fluids, **30**(5), pp. 480–504.
[12] Poujade, O., and Peybernes, M., 2010, "Growth Rate of Rayleigh–Taylor Turbulent Mixing Layers With the Foliation Approach," Phys. Rev. E, **81**(1), p. 016316.
[13] Youngs, D. L., 1984, "Numerical Simulation of Turbulent Mixing by Rayleigh–Taylor Instability," Physica D, **12**(13), pp. 32–44.
[14] Dimonte, G., Youngs, D. L., Dimits, A., Weber, S., Marinak, M., Wunsch, S., Garasi, C., Robinson, A., Andrews, M. J., Ramaprabhu, P., Calder, A. C., Fryxell, B., Biello, J., Dursi, L., MacNeice, P., Olson, K., Ricker, P., Rosner, R., Timmes, F., Tufo, H., Young, Y.-N., and Zingale, M., 2004, "A Comparative Study of the Turbulent Rayleigh–Taylor Instability Using High-Resolution Three-Dimensional Numerical Simulations: The Alpha-Group Collaboration," Phys. Fluids, **16**(5), pp. 1668–1693.
[15] Livescu, D., Wei, T., and Peterson, M. R., 2011, "Direct Numerical Simulations of Rayleigh–Taylor Instability," J. Phys.: Conf. Ser., **318**(082007), pp. 1–10.
[16] Youngs, D. L., 2013, "The Density Ratio Dependence of Self-Similar Rayleigh–Taylor Mixing," Philos. Trans. R. Soc. London, Ser. A, **371**(2003), pp. 1–15.
[17] Dimonte, G., 2000, "Spanwise Homogeneous Buoyancy-Drag Model for Rayleigh–Taylor Mixing and Experimental Evaluation," Phys. Plasma, **7**(6), pp. 2255–2269.
[18] Dimonte, G., Ramaprabhu, P., and Andrews, M., 2007, "Rayleigh–Taylor Instability With Complex Acceleration History," Phys. Rev. E, **76**(4), p. 046313.
[19] Ramaprabhu, P., Karkhanis, V., and Lawrie, A. G. W., 2013, "The Rayleigh–Taylor Instability Driven by an Accel-Decel-Accel Profile," Phys. Fluids, **25**(11), pp. 1–33.
[20] Burlot, A., Gréa, B.-J., Godeferd, F. S., Cambon, C., and Griffond, J., 2015, "Spectral Modelling of High Reynolds Number Unstably Stratified Homogeneous Turbulence," J. Fluid Mech., **765**, pp. 17–44.
[21] Gauthier, S., and Bonnet, M., 1990, "A k–ε Model for Turbulent Mixing in Shock-Tube Flows Induced by Rayleigh–Taylor Instability," Phys. Fluids A, **2**(9), pp. 1685–1694.
[22] Grégoire, O., Souffland, D., and Gauthier, S., 2005, "A Second-Order Turbulence Model for Gaseous Mixtures Induced by Richtmyer–Meshkov Instability," J. Turbul., **6**(29), pp. 1–20.
[23] Llor, A., and Bailly, P., 2003, "A New Turbulent Two-Field Concept for Modeling Rayleigh–Taylor, Richmyers–Meshkov, and Kelvin–Helmholtz Mixing Layers," Laser Part. Beams, **21**(7), pp. 311–315.
[24] Griffond, J., Gréa, B.-J., and Soulard, O., 2015, "Numerical Investigation of Self-Similar Unstably Stratified Homogeneous Turbulence," ASME J. Turbul., **16**(2), pp. 167–183.
[25] Grinstein, F. F., Margolin, L. G., and Rider, W. J., 2007, *Implicit Large Eddy Simulation: Computing Turbulent Fluid Dynamics*, Cambridge University, Cambridge, UK.
[26] Zhou, Y., 2010, "Renormalization Group Theory for Fluid and Plasma Turbulence," Phys. Rep., **488**(1), pp. 1–49.
[27] Lesieur, M., 2008, *Turbulence in Fluids*, Fluid Mechanics and Its Applications Series, Springer, Berlin.
[28] Chen, S., Doolen, G., Herring, J. R., Kraichnan, R. H., Orszag, S. A., and She, Z. S., 1993, "Far-Dissipation Range of Turbulence," Phys. Rev. Lett., **70**(20), pp. 3051–3054.
[29] Canuto, V. M., Dubovikov, M. S., and Dienstfrey, A., 1997, "A Dynamical Model for Turbulence. IV. Buoyancy-Driven Flows," Phys. Fluids, **9**(7), pp. 2118–2131.
[30] Zhou, Y., Robey, H. F., and Buckingham, A. C., 2003, "Onset of Turbulence in Accelerated High-Reynolds-Number Flow," Phys. Rev. E, **67**(5), p. 056305.
[31] Hanazaki, H., and Hunt, J. C. R., 1996, "Linear Processes in Unsteady Stably Stratified Turbulence," J. Fluid Mech., **318**(6), pp. 303–337.
[32] Gréa, B.-J., 2013, "The Rapid Acceleration Model and the Growth Rate of a Turbulent Mixing Zone Induced by Rayleigh–Taylor Instability," Phys. Fluids, **25**(1), p. 015118.
[33] Johnson, B. M., and Schilling, O., 2011, "Reynolds-Averaged Navier–Stokes Model Predictions of Linear Instability. i: Buoyancy- and Shear-Driven Flows," J. Turbul., **12**(36), pp. 1–38.
[34] Mueschke, N. J., and Schilling, O., 2009, "Investigation of Rayleigh–Taylor Turbulence and Mixing Using Direct Numerical Simulation With Experimentally Measured Initial Conditions. II. Dynamics of Transitional Flow and Mixing Statistics," Phys. Fluids, **21**(1), p. 014107.
[35] Schilling, O., 2010, "Rayleigh–Taylor Turbulent Mixing: Synergy Between Simulations, Experiments, and Modeling," 12th International Workshop on the Physics of Compressible Turbulent Mixing, Moscow.
[36] Schilling, O., and Mueschke, N. J., 2010, "Analysis of Turbulent Transport and Mixing in Transitional Rayleigh–Taylor Unstable Flow Using Direct Numerical Simulation Data," Phys. Fluids, **22**(10), p. 105102.

[37] Souffland, D., Soulard, O., and Griffond, J., 2014, "Modeling of Reynolds Stress Models for Diffusion Fluxes Inside Shock Waves," ASME J. Fluids Eng., **136**(9), p. 091102.
[38] Schwarzkopf, J. D., Livescu, D., Gore, R. A., Rauenzahn, R. M., and Ristorcelli, J. R., 2011, "Application of a Second-Moment Closure Model to Mixing Processes Involving Multicomponent Miscible Fluids," ASME J. Turbul., **12**(49), pp. 1–35.
[39] Watteaux, R., 2012, "Détection des grandes structures turbulentes dans les couches de mélange de type Rayleigh–Taylor en vue de la validation de modèles statistiques turbulents bi-structure," Ph.D. thesis, Thèse de doctorat en Science de l'Ecole Normale Supérieure de Cachan, Cachan.
[40] Gréa, B.-J., 2015, "The Dynamics of the $k\ \varepsilon$ Mix Model Toward its Self-Similar Rayleigh–Taylor Solution," ASME J. Turbul., **16**(2), pp. 184–202.
[41] Schiestel, R., 2008, *Modeling and Simulation of Turbulent Flows*, Wiley, New York.
[42] Banerjee, A., Gore, R. A., and Andrews, M. J., 2010, "Development and Validation of a Turbulent-Mix Model for Variable-Density and Compressible Flows," Phys. Rev. E, **82**(4), p. 046309.